



# Evolution of the Dust Composition in Damped Ly $\alpha$ Systems

Giovanni Vladilo<sup>1,2</sup> , Lorenzo Giovannini<sup>2</sup>, Francesca Matteucci<sup>2,3</sup> , and Marco Palla<sup>2</sup><sup>1</sup> INAF—Trieste Astronomical Observatory, Via G.B. Tiepolo 11, I-34143 Trieste, Italy; [vladilo@oats.inaf.it](mailto:vladilo@oats.inaf.it)  
<sup>2</sup> Dipartimento di Fisica, Sezione di Astronomia, Università di Trieste, via G.B. Tiepolo 11, I-34100 Trieste, Italy  
<sup>3</sup> INFN, Sezione di Trieste, Via Valerio 2, I-34100 Trieste, Italy

Received 2018 March 15; revised 2018 October 9; accepted 2018 October 14; published 2018 November 30

## Abstract

We present a method for estimating the relative abundances of refractory elements in the interstellar dust of galaxies hosting damped Ly $\alpha$  (DLA) systems. The method requires gas-phase column densities of volatile and refractory elements, obtained from absorption-line spectroscopy, and interstellar abundances of the same elements, predicted by chemical evolution models of DLA galaxies. We applied this method to the sample of DLA systems with measurements of Mg, Si, S, Fe, and Zn column densities. We find that the dust abundance ratios (Si/Fe)<sub>d</sub> and (Mg/Fe)<sub>d</sub> decrease by almost two orders of magnitude in the metallicity range between  $\simeq 1/100$  solar to roughly solar. This decrease is stronger than the well-known decline of  $\alpha$ /Fe ratios with metallicity observed in metal-poor stars and galaxies, suggesting the existence of metallicity-dependent mechanisms of dust production. To cast light on these mechanisms we investigated the contributions of different stellar sources and interstellar processes to the galactic cycle of dust. We find that Type II SNe are important contributors to the dust composition at low metallicity ( $[\text{Fe}/\text{H}] < -0.6$ ), whereas dust accretion in the interstellar medium appears to be important at higher metallicities, leading to a gradual rise of iron-rich particles, possibly in metal form. To further investigate the nature of the dust, we introduced an idealized model of dust grains based on a mixture of silicates (pyroxenes and olivines) and an iron-rich constituent. The model reproduces the evolutionary trends and suggests that olivines are dominant in silicates, in line with other studies of interstellar dust composition.

*Key words:* dust, extinction – galaxies: evolution – galaxies: ISM – ISM: abundances – quasars: absorption lines

## 1. Introduction

Stellar and interstellar elemental abundances are a key diagnostic tool for probing the origin and evolution of galaxies. For instance, the history of star formation can be constrained by comparing measurements of elemental abundances with predictions of galactic chemical evolution models (Matteucci 2001a, 2001b; Pagel 2009). Since stars form from interstellar clouds, stellar abundances indicate the galactic composition at the time of stellar birth. Interstellar abundances, on the other hand, indicate the galactic composition at the time of the observations. Thanks to this fact, the interstellar abundances of galaxies observed at different ages can be used to directly probe different stages of galactic chemical evolution. Damped Ly $\alpha$  systems (DLAs) provide an ideal tool to pursue this goal, given the fact that these QSO absorbers sample the interstellar medium of galaxies observed in a broad interval of cosmic epochs, back in time to the early stages of their chemical evolution. By definition, DLA systems are characterized by a neutral hydrogen column density  $\log N(\text{H I}) > 20.3$  (Wolfe et al. 1986, 2005), typical of lines of sight intersecting an intervening galaxy. High-resolution spectra of DLAs provide measurements of the chemical composition of galaxies spanning a range of absorption redshift  $1 \lesssim z_{\text{abs}} \lesssim 5$  and a range of metallicities between  $\approx 10^{-3} Z_{\odot}$ , especially at high redshift, up to  $\approx Z_{\odot}$  (e.g., Prochaska et al. 2003; Rafelski et al. 2012; Cooke et al. 2015, 2017). The chemical abundances of DLAs present similarities with those of dwarf galaxies (Matteucci et al. 1997; Calura et al. 2003; Vladilo et al. 2011; Salvadori & Ferrara 2012) and their host galaxies have been associated to the early stages of present-day low-mass galaxies (Møller & Warren 1998; Fynbo et al. 2010; Noterdaeme et al. 2012; Krogager et al. 2013; Christensen et al. 2014).

To infer the chemical composition of DLAs one needs to take into account the impact of dust and ionization effects on the measurements of their elemental abundances (Vladilo 1998; Vladilo et al. 2001). Interstellar dust plays a key role in the interstellar medium (ISM), since it is involved in the formation of molecular hydrogen (Hollenbach & Salpeter 1971; Mathis 1990), the scattering and reddening of stellar light (Draine & Lee 1984; Desert et al. 1990), and the assemblage of solids that drive the formation of rocky bodies in planetary systems (Safronov & Zvjagina 1969; Pollack et al. 1996). The presence of dust grains complicates the measurement of interstellar abundances since the atoms incorporated in the solid phase are not detectable by means of high-resolution optical/UV spectroscopy, the most common technique employed to measure interstellar and DLA abundances. Indeed, the narrow absorption lines observed in high-resolution, optical/UV spectra originate in electronic transitions of atoms in the gas phase, but not in the atoms locked in the dust grains. The lack of detection of the atoms incorporated in the solid phase gives rise to the phenomenon of “elemental depletion,” a deficiency of the gas-phase abundances of refractory elements, recognized since the early studies of local interstellar gas (Spitzer & Jenkins 1975). Interstellar depletions are measured by comparing elemental abundances observed in the gas phase with a proper reference of the total (gas plus dust) abundance; in practice, they indicate which fraction of atoms of an element is locked into dust grains. Elemental depletions have been intensively investigated in the Galactic ISM (Savage & Sembach 1996; Jenkins 2009, 2014) and in DLAs (Hou et al. 2001; Vladilo 2002; Wild et al. 2006; Vladilo et al. 2011; De Cia et al. 2016). In Galactic ISM studies the solar abundances, also called “cosmic abundances,” are used as a reference standard for measuring elemental depletions. In

general, the solar abundance pattern cannot be used in other galaxies and is certainly not appropriate for galaxies observed at different cosmic epochs and different stages of chemical evolution, such as DLA host galaxies. For this reason, models of galactic chemical evolution have been used to provide reference abundance patterns in studies of elemental depletions in DLAs (Vladilo 2002; Calura et al. 2003; Junkkarinen et al. 2004; Vladilo et al. 2006, 2011; De Cia et al. 2013, 2016). In this paper we expand on these types of studies by introducing a method aimed at estimating element-to-element abundance ratios in the dust phase of DLAs.

Elemental depletions do not provide straightforward information about the chemical composition or mineralogy of dust grains (Jones 2014). To infer this type of information, a comparison between astronomical observations and laboratory measurements is necessary (e.g., Agladze et al. 1996; Mennella et al. 1998; Lee 2010; Coupeaud et al. 2011). The available experimental data suggest that interstellar dust consists of carbonaceous species and silicate grains (Draine 2003). The general lack of detection of extinction bump in the spectra of DLAs (Wild & Hewett 2005; Vladilo et al. 2006; York et al. 2006) suggests that the interstellar carbonaceous component is probably weak in DLA host galaxies, or at least in the QSO lines of sight sampled by the observations. On the other hand, direct evidence for the existence of silicates in DLAs has been found in a small sample of dust-rich absorbers (Kulkarni et al. 2007, 2011; Aller et al. 2012, 2014b). Silicon, magnesium, and iron are major constituents of interstellar silicates, which are generally assumed to be made of a mixture of pyroxenes and olivines, even though the chemical structure and the proportion of the mixture is hard to assess. The high depletion factor of iron suggests that this element may also be incorporated in another form of dust, such as metallic particles (e.g., Wickramasinghe & Wickramasinghe 1993; Dwek 2004, 2016; Sofia et al. 2006; Voshchinnikov & Henning 2010; Draine & Hensley 2012, 2013). The aim of this work is twofold: to measure the relative abundance ratios of Si, Mg, and Fe in the dust phase of DLAs, casting light on the nature of the dust, and to search for evolutionary trends of the dust composition as a function of metallicity. To attain these goals we adopt a methodology that combines column-density measurements of refractory and volatile elements with predictions of galactic chemical evolution models. In Section 2 we explain the methodology and in Section 3 we present the resulting abundance ratios in the dust phase, which show clear trends with metallicity. The results are discussed in Section 4: first we explore which stellar sources of dust formation or interstellar processes of dust accretion could be responsible for the trends; then we probe the mineralogy of the dust using a dust grain model featuring a mixture of silicates and an iron-rich, non-silicate component. To the best of our knowledge, this is the first investigation on the ISM of high-redshift galaxies that explores the mineralogy of the dust and its evolution with metallicity. The conclusions are summarized in Section 5.

## 2. Method

To obtain the dust abundance ratios in the ISM of DLA systems, we compare measurements of gas-phase column densities with total ISM abundances predicted by galactic evolution models tailored for DLA systems. We make a distinction between volatile elements, which are assumed to be

mostly in the gas phase, and refractory elements, which are partly locked in the solid component (Spitzer & Jenkins 1975; Savage & Sembach 1996). Refractory elements are characterized by relative high condensation temperatures, i.e., the temperature at which 50% of the element is removed from the gas phase in a cooling gas of solar composition (e.g., Lodders 2003). Refractory elements show significant depletions in local ISM studies, in line with the expectation that they are readily incorporated in the dust component. Volatile elements have low condensation temperatures and are characterized by very weak depletions, indicating that they tend to stay in the gas phase. In the rest of this section, we describe how to make use of the specific properties of volatile and refractory elements for deriving the equations of the method; we then explain how to take advantage of previous studies of galactic chemical evolution to build a model tailored for DLA host galaxies.

### 2.1. Dust Abundance Ratios

Let us call  $N_i^{\text{ISM}}$  the total column density of an element  $i$  in the ISM. Since part of its abundance resides in the gas phase of the ISM, whereas the rest is incorporated in the dust phase, the total column density can be expressed as follows:

$$N_i^{\text{ISM}} = N_i^g + N_i^d, \quad (1)$$

where the first and the second terms on the right side of the equation indicate the gas and dust phase contributions, respectively. For a refractory element,  $i = R$ , we can write:

$$N_R^{\text{ISM}} = N_R^g + N_R^d. \quad (2)$$

For an ideal volatile element,  $i = V$ , no abundance in the dust phase is expected and therefore the total column density in the ISM is equal to the one measured in the gas phase:

$$N_V^{\text{ISM}} = N_V^g \equiv N_V. \quad (3)$$

By combining Equations (2) and (3) we obtain

$$N_R^d = N_V (N_R/N_V)^{\text{ISM}} - N_R^g, \quad (4)$$

where  $(N_R/N_V)^{\text{ISM}}$  is the total abundance ratio between the refractory and the volatile element. For two refractory elements,  $R_1$  and  $R_2$ , the average abundance ratio in the dust along the DLA sight line will be

$$\left( \frac{N_{R_1}}{N_{R_2}} \right)^d = \frac{N_V (N_{R_1}/N_V)^{\text{ISM}} - N_{R_1}^g}{N_V (N_{R_2}/N_V)^{\text{ISM}} - N_{R_2}^g}. \quad (5)$$

This expression can be solved by inserting the gas-phase column densities  $N_{R_1}$ ,  $N_{R_2}$ , and  $N_V$  measured from optical/UV absorption spectroscopy; concerning the total abundance ratios,  $(N_{R_1}/N_V)^{\text{ISM}}$  and  $(N_{R_2}/N_V)^{\text{ISM}}$ , we adopt the predictions of models of galactic chemical evolution tuned for DLA systems, as we explain below. Since Equation (5) depends on the column density of a single volatile element, we can choose the most appropriate volatile element according to available data set: for instance, the element with the smallest measurement error, or the element that is observable for a given instrumental configuration and a specific absorption redshift. Details on the adopted volatile elements are given in Section 3.

### 2.1.1. Error Analysis

To estimate the measurement error of the ratio  $(N_{R_1}/N_{R_2})^d$  we rewrite Equation (5) as:

$$\rho = \frac{ax - y}{bx - z}, \quad (6)$$

where  $\rho \equiv (N_{R_1}/N_{R_2})^d$ ;  $x$ ,  $y$ , and  $z$  indicate the measured quantities  $N_V$ ,  $N_{R_1}$ ,  $N_{R_2}$ , respectively;  $a$  and  $b$  refer to the model predictions  $(N_{R_1}/N_V)^{\text{ISM}}$  and  $(N_{R_2}/N_V)^{\text{ISM}}$ , respectively, which are not considered in the error propagation. To estimate the error propagation on the variable  $\rho$ , we define  $u \equiv ax - y$  and  $v \equiv bx - z$ , obtaining

$$\sigma_\rho = \frac{1}{v^2} \sqrt{(av - bu)^2 \sigma_x^2 + v^2 \sigma_y^2 + u^2 \sigma_z^2}. \quad (7)$$

We use this expression to reject low-quality data observational data: the measurement of the ratio calculated with Equation (5) is rejected if  $\sigma_\rho > \sigma_{\text{lim}}$ , where we adopt  $\sigma_{\text{lim}} = 0.5$  dex as the limiting error. The impact of the systematic uncertainties of  $a$  and  $b$ , which are related to the adoption of a specific model of galactic chemical evolution, can be assessed by repeating the calculations of the chemical evolution model for different sets of parameters.

At variance with the assumption of Equation (3), no element is completely volatile. This fact will introduce a systematic error in the derivation of dust abundance ratios with Equation (5). To estimate the impact of this effect we proceed as follows. We call  $f_V = N_V^d / (N_V^g + N_V^d)$  the (small) fraction of the volatile element that is locked into dust grains; the total column density in the medium becomes

$$N_V^{\text{ISM}} = N_V^g (1 + \epsilon_V), \quad (8)$$

where  $\epsilon_V = f_V / (1 - f_V)$ , and the dust column-density ratio can be expressed as

$$\left( \frac{N_{R_1}}{N_{R_2}} \right)^d = \frac{N_V (1 + \epsilon_V) (N_{R_1}/N_V)^{\text{ISM}} - N_{R_1}^g}{N_V (1 + \epsilon_V) (N_{R_2}/N_V)^{\text{ISM}} - N_{R_2}^g}. \quad (9)$$

The absolute difference between the results obtained from Equations (9) and (5) is adopted as an estimate of the systematic error potentially introduced by the presence of a small amount of depletion of the volatile element. Cases in which the systematic error estimated in this way exceed the statistical error calculated with Equation (7) are rejected. In practice, a range of values of  $\epsilon_V$  is explored, based on the properties of the volatile elements known from ISM studies. Details on the adopted values of  $\epsilon_V$  are given in Section 3.

## 2.2. Galactic Chemical Evolution Model

To estimate the total abundances in the ISM of DLA systems we use the model of galactic chemical evolution presented by Giovannini et al. (2017b). Here we briefly summarize the model prescriptions, which have been tuned for DLA host galaxies. We refer the reader to the original paper for details.

We call  $G_i(t) = M_{\text{ISM}}(t)/M_{\text{ISM}}(t_G)$  the ratio of the mass of an element  $i$  in the ISM at the time  $t$  over the total gas mass at the present time  $t_G$ . The evolution of  $G_i(t)$  depends on how the gas is processed during the cosmic time and can be described by

the following equation:

$$\dot{G}_i(t) = -\dot{G}_i^{\text{SFR}} + \dot{G}_i^{\text{production}} + \dot{G}_i^{\text{infall}} - \dot{G}_i^{\text{wind}}. \quad (10)$$

The first term on the right side of the Equation (10),  $\dot{G}_i^{\text{SFR}} = -\psi(t)X_i(t)$ , represents the fraction of an element  $i$  removed from the gas by star formation, where  $\psi(t)$  is the star formation rate (SFR) and  $X_i(t) = G_i(t)/G(t)$  is the abundance by mass. We assume that the SFR is proportional to the mass of the gas present in the galaxy, by using the characteristic Schmidt law (Schmidt 1959):

$$\psi(t) = \nu G(t), \quad (11)$$

where  $\nu$ , in units of  $\text{Gyr}^{-1}$ , is the star formation efficiency and expresses the rate at which stars form.

The second term of Equation (10)  $\dot{G}_i^{\text{production}}$  represents the rate at which the mass fraction of the element  $i$  is restored into the ISM by stars. This term takes into account the chemical enrichment of single low and intermediate-mass stars (LIMS,  $0.8 < m_*/M_\odot < 8$ ), core collapse SN explosions of massive stars ( $8 < m_*/M_\odot < 80$ ) and Type Ia SNe, for which we assume the single-degenerate scenario (Whelan & Iben 1973; Matteucci & Recchi 2001).

The mass and the chemical composition injected into the ISM by a stellar population depends on the adopted stellar yields, which represent the amount of both newly formed and pre-existing elements injected into the ISM by stars at their death. In this work, we adopt the stellar yields from van den Hoek & Groenewegen (1997) for LIMS, the yields from François et al. (2004) for stars with mass  $> 8 M_\odot$ , and Iwamoto et al. (1999) for Type Ia SNe. The third term on the right side of Equation (10) accounts for the infalling material that accretes onto the galaxy: in fact, we consider our galaxy to form by the accretion (gravitational collapse) of a cloud of primordial chemical composition in a pre-existing diffuse dark matter halo. We adopt an exponential law for the infall, with the characteristic timescale  $\tau_{\text{inf}}$ :

$$\dot{G}_i^{\text{infall}} = X_{i,\text{infall}} e^{-t/\tau_{\text{inf}}}. \quad (12)$$

The last term in Equation (10) represents the element mass fraction removed from the ISM by the galactic wind. The galactic wind is assumed proportional to the SFR and it starts when the gas thermal energy, heated by SN explosions, exceeds the gravitational binding energy of the system. The parameter  $\omega$ , represents the efficiency of the wind, and it is assumed constant for all the elements:

$$\dot{G}_i^{\text{wind}} = \omega \psi(t). \quad (13)$$

Another important quantity of the model is the stellar initial mass function (IMF), which represents the mass distribution of stars at birth in a stellar population. In this work, the IMF is assumed to be constant in space and time and normalized to unity in the total mass interval considered. In particular we adopt a single slope IMF (Salpeter 1955):

$$\phi_{\text{Salp}}(m) = 0.17 m^{-(1+1.35)}. \quad (14)$$

Thanks to previous work, we can tune the parameters of the chemical evolution model specifically for DLA systems: generally, these systems are associated with low-mass and low-luminosity galaxies (e.g., Møller & Warren 1998; Christensen et al. 2014) that experienced low star formation episodes. By studying the chemical

**Table 1**

Parameters of Galactic Chemical Evolution Models Adopted to Reproduce the ISM Abundances of DLA Systems

Parameter	This Work	V11
$T_{\text{infall}}$ (Gyr)	1	1
$M$ ( $10^9 M_{\odot}$ )	5	1, 5
$\nu$ ( $\text{Gyr}^{-1}$ )	0.05	0.05, 0.1, 0.2
$\omega$	3.5	2.0, 3.5, 5.0
IMF	Salpeter	Salpeter

**Note.** First to last row: infall time, mass of the galaxy, star formation efficiency, wind parameter, and initial mass function. Second column: parameters adopted in the present work. Third column: parameters adopted in a comparison test with 18 models of dwarf irregulars tuned for DLA systems taken from Vladilo et al. (2011).

composition of DLA systems, many previous investigations associated these objects with dwarf irregular galaxies (e.g., Matteucci et al. 1997; Calura et al. 2003; Vladilo et al. 2011; Cooke et al. 2015). Our parameters are similar to the ones adopted by Vladilo et al. (2011): in that work, they performed a fine tuning of the model by producing a grid of chemical evolution models, where the total mass  $M_{\text{infall}}$ ,  $\nu$  and  $\omega$  were let to vary. Then, they selected the best model by comparison with the observed abundance of volatile elements in DLA systems, on the basis of a least squares method (we refer the reader to the cited article for more details). At variance with Vladilo et al. (2011), we also performed some tests on the variation of the IMF and the timescale of infall, which did not produce substantial differences. In Table 1 we report the parameters of the chemical evolution model adopted in the present work. These values agree with the ones of a typical dwarf irregular galaxy, namely, characterized by a low infall mass and a low star formation efficiency (Bradamante et al. 1998; Recchi et al. 2002; Calura et al. 2008; Gioannini et al. 2017b).

### 3. Results

As a first application of the method we consider the refractory elements Si, Mg, and Fe, which compose the bulk of interstellar silicates, and the volatile elements Zn and S, already employed as undepleted tracers of metallicity in previous studies of DLA abundances. The inclusion of Fe in this study is important to test whether or not iron could also be incorporated in a form different from silicates. Thanks to the fact that the number of DLA column-density measurements is relatively high for Si, Fe, Zn, and S, we can build a sample of dust abundance ratios sufficiently large to search for evolutionary trends. Unfortunately, the number of Mg column densities is relatively small, because the only unsaturated lines of Mg II that are found in DLAs belong to an extremely weak doublet that lies in the Ly $\alpha$  forest of the quasar spectrum. Even so, Mg data are very important to discriminate the chemical composition of silicates, which may appear in Mg-rich or Mg-poor compounds.

Since only one volatile element is required to estimate the dust abundance ratio of two refractories with Equation (5), the use of both Zn and S helps to enlarge the sample, because Zn is better observed at relatively low redshift, whereas S is better observed at high redshift. The choice of these two volatile elements is also justified by the fact that the stellar yields of Zn and S, used in the model of galactic evolution, are more robust than those of other volatiles, such as P. For a discussion of the caveats related to the use of S and Zn as volatile interstellar

elements we refer the reader to Jenkins (2009) and Vladilo et al. (2011). To estimate the systematic error due the potential presence of a small depletion of S and Zn, we used Equation (9). We tested the impact of  $\epsilon_{\text{Zn}}$  and  $\epsilon_{\text{S}}$  values in the range of 0.1–0.25 dex, based on the depletions provided by De Cia et al. (2016) for low-metallicity environments. As we did not find substantial differences in this range, we adopted  $\epsilon_{\text{Zn}} = \epsilon_{\text{S}} = 0.1$  dex in the estimate of the systematic errors. Cases in which this error exceeded the statistical error (7) by 0.15 dex were discarded.

Concerning the ISM abundances  $(N_{R_i}/N_V)^{\text{ISM}}$  that appear in Equation (5), we adopted the total abundance ratios (gas plus dust) Si/Zn, Si/S, Mg/Zn, Mg/S, Fe/Zn, and Fe/S predicted by the models of galactic chemical evolution presented above (Section 2.2). Since these models have been constrained using ratios of volatile elements, such as the S/Zn ratio, their predictions are not influenced by the properties of the dust, which would instead affect refractory elements. In addition, the total ISM abundance ratios predicted by these models do not depend on the recipes that describe the production and growth of the dust: these recipes are used at a later stage of our analysis to assess which processes could be responsible for the formation and evolution of the dust (Section 4.1). In practice, once a reference galactic chemical evolution model is adopted, the total ISM abundance ratios of interest,  $(N_{R_i}/N_V)^{\text{ISM}}$ , are calculated at the value of metallicity measured in each DLA system and inserted in Equation (9) together with the relevant gas-phase column densities obtained from the observations.

In Figure 1, we present the dust abundance ratios  $(\text{Si}/\text{Fe})_{\text{d}}$  and  $(\text{Mg}/\text{Fe})_{\text{d}}$  calculated with our method. The column densities used to derive these data are listed in Table 2 of Gioannini et al. (2017b), with Mg II data taken from the compilation of Vladilo et al. (2011). The data are plotted as a function of absolute metallicity, expressed as  $[\text{Zn}/\text{H}]$  or  $[\text{S}/\text{H}]$ , depending on which of the two volatiles has been used to compute the dust abundance ratio. The solar reference values for the absolute metallicities were taken from Asplund et al. (2009).

The left panel of Figure 1 shows that the  $(\text{Si}/\text{Fe})_{\text{d}}$  ratios tend to decrease with metallicity, with a decline of almost two orders of magnitude in the metallicity range between  $\simeq -2.5$  dex and solar. The right panel of the same figure shows the existence of a similar trend for the  $(\text{Mg}/\text{Fe})_{\text{d}}$  ratios, even if in this case there is a much lower amount of data and a lower interval of metallicities is covered, due to the paucity of Mg II column densities. To ascertain the statistical strength of these trends we performed a linear regression to the data and calculated the Pearson correlation coefficients. The linear fits for the DLA sample with Zn column densities are shown in Figure 1 (dashed lines). The parameters of the fit are:

$$\left(\frac{N_{\text{Si}}}{N_{\text{Fe}}}\right)^{\text{d}} = -0.54_{\pm 0.05} [\text{Zn}/\text{H}] - 0.42_{\pm 0.04}$$

$$\left(\frac{N_{\text{Mg}}}{N_{\text{Fe}}}\right)^{\text{d}} = -0.47_{\pm 0.26} [\text{Zn}/\text{H}] - 0.53_{\pm 0.24},$$

with Pearson correlation coefficients  $r = -0.78$  and  $r = -0.62$  for  $(N_{\text{Si}}/N_{\text{Fe}})^{\text{d}}$  and  $(N_{\text{Mg}}/N_{\text{Fe}})^{\text{d}}$ , respectively. The slopes of the two trends are similar, at least within the large uncertainties of the smaller sample of  $(\text{Mg}/\text{Fe})_{\text{d}}$  ratios. This similarity is

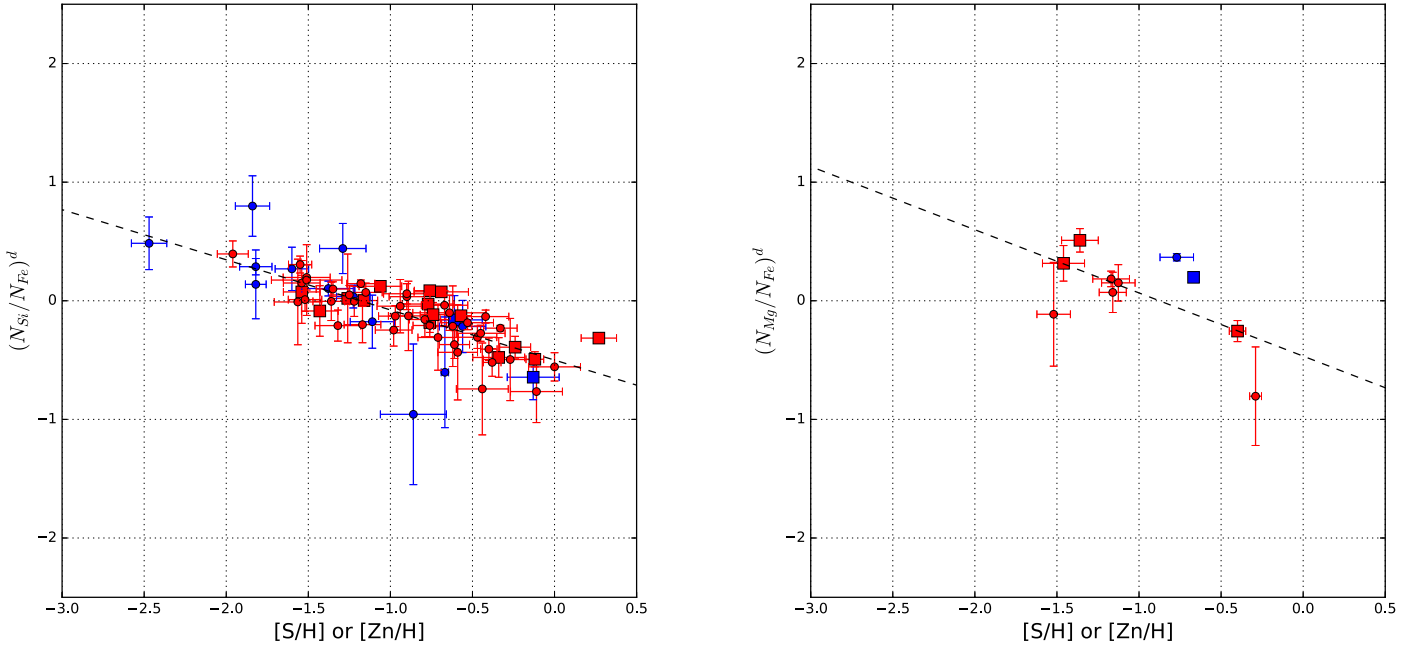


**Figure 1.** Dust abundance ratios  $(\text{Si}/\text{Fe})_d$  (left panel) and  $(\text{Mg}/\text{Fe})_d$  (right panel) in DLA systems derived with Equation (5). The data are plotted as a function of the absolute abundance of Zn or S, which is a dust-free indicator of the metallicity level. Red and blue dots: data for which only the DLA measurement of Zn or S was available, respectively. Red and blue squares: data for which both volatiles measurements were available and the propagated error was lower in the case of Zn or S, respectively. Error bars have been computed with Equation (7). Dashed line: linear regression vs.  $[\text{Zn}/\text{H}]$  of the dust abundance ratios.

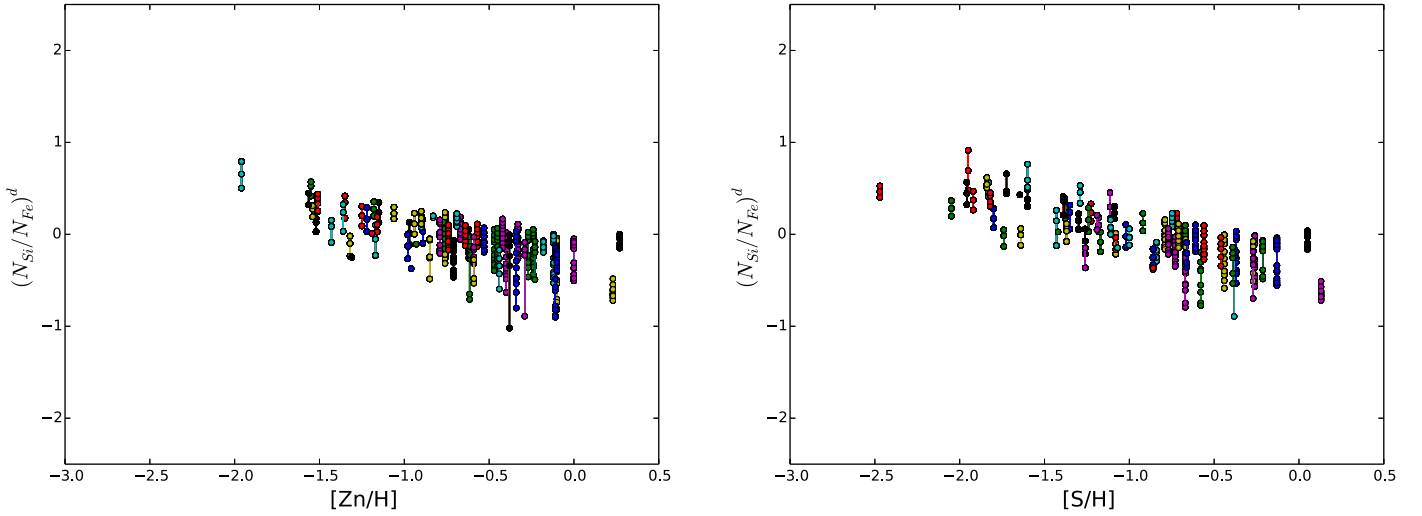


**Figure 2.** Scatter of dust abundance ratios  $(\text{Si}/\text{Fe})_d$  obtained from Equation (5) by adopting different models of chemical evolution for each individual DLA system. The model prescriptions and the range of parameters adopted are summarized in Table 1. The results obtained for the samples of DLA systems with Zn and S column densities are displayed in the left and right panels, respectively. Error bars obtained from Equation (7) have been omitted for the sake of clarity.

consistent with a rise of the relative abundance of iron in the solid-phase component in the course of galactic chemical evolution.

The trends shown in Figure 1 are weakly affected by different choices of the models of galactic evolution, as long as the models are constrained with the properties of DLA galaxies and tuned with the S/Zn ratio. This is due to the fact that, with such constraints, the ratios  $(N_{R_i}/N_V)^{\text{ISM}}$  share a similar dependence on metallicity. To quantify how the estimates of the  $(\text{Si}/\text{Fe})_d$  ratios can be affected by the adoption of different models of galactic chemical evolution we performed a comparison test with models previously tuned to fit the S/Zn ratio in DLA systems. Specifically, we varied the mass of the galaxy, the star formation efficiency, and the strength of the galactic wind of the models of dwarf irregular galaxies

described in Vladilo et al. (2011). The range of parameters adopted in this test are listed in the last column of Table 1 and the results are shown in Figure 2. For each DLA system, the scatter of the ratios at each value of  $[\text{Zn}/\text{H}]$  (left panel) or  $[\text{S}/\text{H}]$  (right panel) is representative of the uncertainty introduced by the adoption of the different models. The standard deviation of the  $(\text{Si}/\text{Fe})_d$  ratios found for each DLA system is generally smaller than the error bar estimated with Equation (7) for a single model. The trend of decreasing ratios with increasing metallicity is recovered with all models, both using Zn (left panel) and S (right panel) as the volatile elements of reference. These results suggest that the decrease with metallicity of the  $(\text{Si}/\text{Fe})_d$  and  $(\text{Mg}/\text{Fe})_d$  ratios is not an artifact resulting from a particular choice of the models of galactic evolution.

The decrease of the  $(\text{Si}/\text{Fe})_d$  ratios, and probably of the  $(\text{Mg}/\text{Fe})_d$  ratios, indicates that the dust chemical composition of DLA galaxies varies with metallicity and therefore with the stage of galactic chemical evolution. Since each point in Figure 1 corresponds to an individual DLA galaxy, the existence of a common trend suggests that DLA galaxies share a common evolution of dust composition, at least as far as the Si/Fe and Mg/Fe ratios are concerned. Quite remarkably, we are not able to test whether or not a trend of this type has existed in the course of the chemical evolution of our own Galaxy, given the fact that we do not have a way to probe the past properties of the Milky Way interstellar dust. This fact emphasizes the importance of the trend shown in Figure 1 and confirms the remarkable potential of DLA absorption-line observations for studies of chemical evolution.

The strong decrease of the  $(\text{Si}, \text{Mg})/\text{Fe}$  ratios that we find in the dust phase of DLA systems should not be confused with the weaker decrease with the metallicity of the  $\alpha/\text{Fe}$  ratios found in low-metallicity stars and galaxies. For instance, the  $(\text{Si}, \text{Mg})/\text{Fe}$  ratios in metal-poor stars and galaxies decrease by only  $\approx 0.2$  dex in the metallicity range of  $[-2.0, 0.0]$ . This trend is a known feature confirmed by both observations (e.g., Lu et al. 1996; Cooke et al. 2011; Rafelski et al. 2012; Cooke et al. 2015) and chemical evolution models (e.g., Kunth et al. 1995; Matteucci et al. 1997; Calura et al. 2003; Spitoni et al. 2009), and is attributed to the delayed pollution in the ISM of iron with respect to  $\alpha$ -capture elements.<sup>4</sup> Despite the significant difference in strength, it is remarkable that the trend of the dust composition follows the same direction of the trend of the total abundances: this fact suggests that the evolution of the dust composition is connected, to some extent, to the injection of the elements in the ISM. For instance, a very simple interpretation of the trend of the dust composition would be that iron-rich dust might become important at late stages of evolution, when more and more iron is injected in the ISM through Type Ia SNe. However, the quantitative interpretation of the element-to-element ratios in the dust is more complex than this: as we discuss in the next section, the dust abundance ratios depend on the relative contributions of different dust sources (AGB stars, Type II SNe, and dust growth) and on the types of dust grains present in the ISM.

#### 4. Discussion

The evolutionary trends of dust composition presented in Section 3 are based on a combination of measurements and model predictions. Ideally, it would be nice to test these results with direct observations of the dust component of the host galaxies of DLA systems. However, direct observations of this type are very challenging due to the proximity of the faint host galaxy to the bright background QSO (Le Brun et al. 1997; Rao et al. 2003; Kulkarni et al. 2006; Fumagalli et al. 2015). The application of integral field unit (IFU) techniques provides information on the redshift, metallicity, and SFRs of the host galaxies (Péroux et al. 2011; Bouché et al. 2012; Bielby et al. 2017; Fumagalli et al. 2017; Rahmani et al. 2018) rather than on their dust composition. Direct measurements of silicate absorptions in DLAs do exist, but only for a very limited sample of dust-rich absorbers (Kulkarni et al. 2007, 2011; Aller et al. 2012, 2014b). Given this challenging observational scenario, we should at least provide a way to

interpret the observed evolutionary trends of dust composition. To this end we proceed with two distinct approaches. First we investigate which stellar sources of dust and/or interstellar processes of dust accretion may explain the observed trends. Then we test the capability of a simple model of dust grains to reproduce the same trends.

##### 4.1. The Dust Cycle in DLA Host Galaxies

In this section we compare the evolutionary trends of dust composition presented in Figure 1 with a model of galactic evolution that describes the production of dust by different sources (Type II SNe, AGB stars, and dust growth/accretion in the ISM). The galactic evolution model is the same one used to calculate the mass of individual elements in the ISM normalized to the infall mass,  $G_i$ . Since these quantities do not bear information on the dust depletion, we consider, in addition, the mass fraction of individual element locked in the dust,  $G_{i,\text{dust}}$ . The temporal evolution of this quantity can be expressed as

$$\begin{aligned} \dot{G}_{i,\text{dust}}(t) = & -\psi(t)X_{i,\text{dust}}(t) + \delta_i R_i(t) + \left( \frac{G_{i,\text{dust}}(t)}{\tau_{\text{accretion}}} \right) \\ & - \left( \frac{G_{i,\text{dust}}(t)}{\tau_{\text{destruction}}} \right) - \omega \cdot X_{i,\text{dust}}(t). \end{aligned} \quad (15)$$

The first term on the right side of this equation represents the amount of dust removed from the ISM due to star formation, the second represents the injection in the ISM of new dust from stellar sources (Type II SNe and AGB stars, and the third and the fourth terms represent the dust accretion and destruction in the ISM, whereas the last term the dust removal by galactic wind. The galactic wind may decrease the total mass in dust (Gioannini et al. 2017b), but does not affect significantly the abundance ratio of different elements in the dust phase. Based on recent observational data and theoretical studies we do not include Type Ia SNe among the potential sources of dust: most of the observations obtained with the *Spitzer* and *Herschel* satellites indicate that the infrared emission from Type Ia SN remnants originates in shocked interstellar dust rather than in newly formed dust (Blair et al. 2007; Gomez et al. 2012; Williams et al. 2012); recent theoretical studies indicate that that dust formed in Type Ia SN explosions is destroyed before it can be injected into the ISM (Nozawa et al. 2011).

With the addition of the above equation, the galactic evolution model is able to trace the dust evolution in the ISM taking into account all the processes contributing to the “dust cycle,” in a way similar to that followed in previous work (Dwek 1998; Calura et al. 2008; Zhukovska et al. 2008; Zhukovska 2014). Here we adopt the same prescriptions for dust production already used in the case of dwarf irregular galaxies and DLA systems (Gioannini et al. 2017b), but also tested in galaxies of different morphological type (see Gioannini et al. 2017a; Spitoni et al. 2017). These prescriptions can be summarized as follows. The incorporation into dust of individual elements is described by means of the condensation efficiencies,  $\delta_i$ , which represent the fraction of the element  $i$  expelled from a star that condenses into solid particles. Each condensation efficiency depends on the mass and the metallicity of the stars polluting the ISM. In practice, we adopted the values of  $\delta_i$  reported by Piovan et al. (2011). As far as AGB stars are concerned the adopted condensation

<sup>4</sup> The  $\alpha$ -capture elements are formed by massive stars ( $M_* > 10 M_\odot$ ) by subsequent addition of  $\alpha$ -particles, such as O, Mg, Si, S, and Ca.

**Table 2**Dust Prescriptions in the Chemical Evolution Models Adopted to Reproduce the Dust Abundance Ratios (Si, Mg/Fe)<sub>d</sub> in DLA Systems

Model	Dust Production	Dust Accretion
DLA	P11, $\delta_{i,Fe}$	A13, $\tau_{\text{accr,Fe}}$
DLA na	P11, $\delta_{i,Fe}$	No accretion
DLA t3	P11, $\delta_{i,Fe}$	A13, $\tau_{\text{accr,Fe}}/3.0$
DLA d1.5 t3	P11, $\delta_{i,Fe} \cdot 1.5$	A13, $\tau_{\text{accr,Fe}}/3.0$
DLA d3 t3	P11, $\delta_{i,Fe} \cdot 3.0$	A13, $\tau_{\text{accr,Fe}}/3.0$
DLA t5	P11, $\delta_{i,Fe}$	A13, $\tau_{\text{accr,Fe}}/5.0$
DLA t7	P11, $\delta_{i,Fe}$	A13, $\tau_{\text{accr,Fe}}/7.0$

**Note.** Second column: dust production by stellar ejecta with condensation efficiencies from P11 (Piovan et al. 2011); cases with enhanced condensation efficiencies for iron are indicated. Third column: dust accretion in the ISM with accretion timescales from A13 (Asano et al. 2013); cases with enhanced accretion rates for iron are indicated. The prescriptions for dust destruction are from A13 in all models.

efficiencies are shown in Figure 1 of Gioannini et al. (2017b) as a function of stellar mass and metallicity. For Type II SNe we adopted a neutral hydrogen column density of  $n_{\text{H}} = 0.1 \text{ cm}^{-3}$  for the ambient gas surrounding the explosion, based on the comparison with studies of dust-to-gas ratios in dwarf irregular galaxies (Gioannini et al. 2017a). Concerning the dust processes of accretion and destruction in the ISM, we calculate the metallicity-dependent  $\tau_{\text{accretion}}$  and  $\tau_{\text{destruction}}$  as in Asano et al. (2013), where  $\tau_{\text{accretion}}$  depends on the temperature  $T$ , density  $n_{\text{H}}$ , metallicity  $Z$ , and size of the grains  $a$ :

$$\tau_{\text{accretion}} \propto a^{-1} n_{\text{H}}^{-1} Z^{-1} T^{-1}. \quad (16)$$

The reference value of hydrogen density is high in this case,  $n_{\text{H}} = 100 \text{ cm}^{-3}$ , since the accretion is assumed to take place in dense gas; the other reference values are  $a = 0.1 \mu\text{m}$ ,  $Z = 0.02$ , and  $T = 50 \text{ K}$ . Based on the study of Zn/Fe and S/Fe ratios shown in Figure 11 of Gioannini et al. (2017b), we considered cases with increased rates of iron accretion. To reproduce the dust abundance ratios (Si/Fe)<sub>d</sub> and (Mg/Fe)<sub>d</sub> seen in Figure 1 we also explored different values of iron condensation efficiencies. The specific prescriptions of the dust production models are summarized in Table 2. The corresponding model predictions are shown in Figure 3 (curves with different colors) on top of the DLA ratios estimated with Equation (5) (black diamonds with error bars). The yellow line represents the predictions obtained by increasing the iron accretion rate by a factor of 3. This line shows a moderate decrease at low metallicities ( $[\text{Fe}/\text{H}] < -0.7$ ) followed by a steeper decrease at higher metallicities ( $-0.7 < [\text{Fe}/\text{H}] < 0.5$ ). The change of slope is caused by the varying contributions of different dust processes in the course of the evolution. At low metallicities, dust production from Type II SNe is the most important process of dust formation. These SNe produce mainly  $\alpha$ -capture elements and only a small fraction of Fe. This characteristic, together with the typical short timescales of the massive progenitors (shorter than 30 Myr for stars with masses  $M_{*} > 8 M_{\odot}$ , e.g., Padovani & Matteucci 1993), leads to the typical high values of  $\alpha/\text{Fe}$  ratios observed in low-metallicity environments (e.g., Matteucci et al. 1997; Calura et al. 2003; Spitoni et al. 2016). As we said, the dust composition also shows a decrease of the  $\alpha/\text{Fe}$  ratios with

increasing metallicity, but with a much steeper slope than that observed in low-metallicity environments. The values of the (Si/Fe)<sub>d</sub> and (Mg/Fe)<sub>d</sub> ratios predicted with the model of dust production depend on the adopted dust condensation efficiencies,  $\delta_i$ . To assess the impact of this parameter we changed the iron condensation efficiency from Type II SNe,  $\delta_{\text{Fe}}^{\text{II}}$ , at constant iron accretion rate (see Table 2): the cyan and blue lines were obtained by increasing  $\delta_{\text{Fe}}^{\text{II}}$  by factors 1.5 and 3.0, respectively (we checked that the increased values of  $\delta_{\text{Fe}}^{\text{II}}$  remain  $\leq 1.0$ , in agreement with the definition of condensation efficiency). As we expected, as the  $\delta_{\text{Fe}}^{\text{II}}$  increases, both ratios (Si/Fe)<sub>d</sub> and (Mg/Fe)<sub>d</sub> decrease, indicating that the variation of the dust abundance ratios at low metallicities is strictly connected to dust production by Type II SNe. The variation of  $\delta_{\text{Fe}}^{\text{II}}$  significantly affects the results at low metallicity, whereas the three models with constant accretion rate and increasing  $\delta_{\text{Fe}}$  almost trace each other at higher metallicities. The reason is that at high metallicities dust growth in the ISM becomes more important than dust formation from Type II SNe; as a result, the (Si, Mg/Fe)<sub>d</sub> ratios become almost independent of the condensation efficiencies of Type II SNe. In general, our analysis indicates that dust growth is a fundamental process of the dust cycle in galaxies, especially at high metallicity. This conclusion can be appreciated in Figure 3, where we show the impact of different values of dust growth on the predictions of the galactic evolution model. The green-dotted line shows what happens without dust growth: no significant decrease of (Si, Mg/Fe)<sub>d</sub> is predicted, in complete disagreement with the ratios estimated with our method. The black dashed-dotted line shows the case with the accretion rate taken at face value from Asano et al. (2013): after an initial decrease at low metallicity the model predicts a constant value of (Si/Fe)<sub>d</sub> and (Mg/Fe)<sub>d</sub>, which is still in disagreement with the data. The red and magenta lines represent models with more efficient Fe-rich dust growth, i.e., models with a shorter timescale for Fe growth as indicated in the legend and in Table 2. Models with shorter timescales for Fe-rich dust growth tend to provide a better agreement with the results presented in Section 3. According to Equation (16), all the other ISM conditions being constant, a shorter timescale implies a smaller size of dust grains. The better agreement obtained with higher dust growth is consistent with the existence of iron-rich interstellar dust grains with sizes smaller than  $0.1 \mu\text{m}$ . A similar conclusion was presented in Gioannini et al. (2017b).

The fact that iron accretion is required to fit the data in Figure 3 favors a scenario where a significant fraction of iron in DLA galaxies is in the form of free-flying particles that can accrete iron atoms from the gas phase. Studies of the galactic interstellar dust suggest a combination of free-flying iron with variable amounts of iron locked inside a matrix of silicates (Jones et al. 2013; Zhukovska et al. 2018). Indirect evidence for the existence of a free form of interstellar iron is provided by the detection of troilite (FeS) in star dust collected in the solar system (Zolensky et al. 2006) and in dust grains in protoplanetary disks (Keller et al. 2002): should all iron be locked inside silicates, the formation of troilite would not be possible; only iron in free form could interact with sulfur and generate FeS.

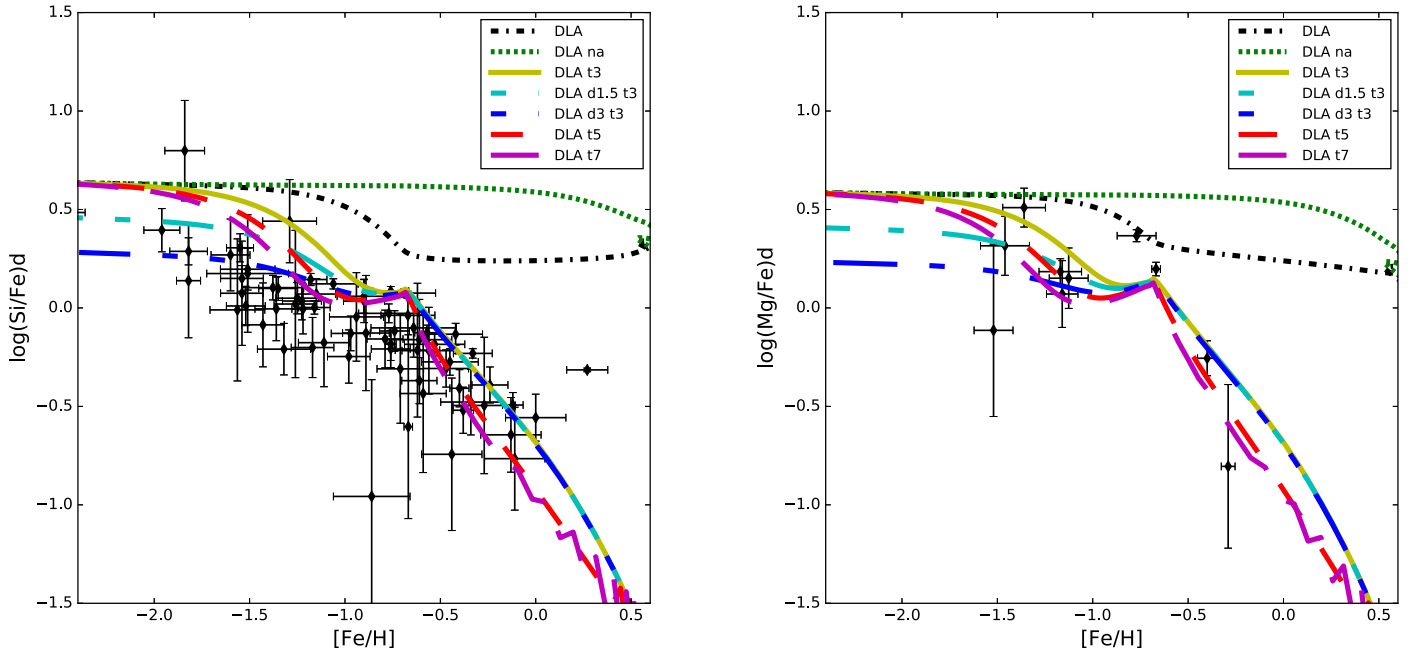


**Figure 3.** Comparison of the dust abundance ratios  $(\text{Si}/\text{Fe})_d$  and  $(\text{Mg}/\text{Fe})_d$  shown in Figure 1 (diamonds with error bars) with models of dust production by stellar ejecta and interstellar accretion (curves with different colors). Starting from the reference model of [Gioannini et al. \(2017b\)](#) different recipes for incorporation of iron in dust have been considered. See Table 2 for a summary of the parameters of the models listed in the legend.

#### 4.2. Nature and Evolution of Dust Grains

The  $(\text{Si}/\text{Fe})_d$  and  $(\text{Mg}/\text{Fe})_d$  ratios derived with our method can be used to cast light on the nature and evolutionary properties of dust grains. With this aim in mind we introduce an idealized model of dust grain composition. The “graphite and silicate” model ([Hoyle & Wickramasinghe 1969](#)) was the basis of most subsequent dust grain composition models ([Mathis et al. 1977](#); [Draine & Lee 1984](#); [Desert et al. 1990](#); [Li & Draine 2001](#)). In addition to carbonaceous and silicate components, previous interstellar studies have suggested the existence of iron-rich species, possibly in metallic form ([Dwek 2004](#); [Ueda et al. 2005](#); [Sofia et al. 2006](#); [Voshchinnikov & Henning 2010](#); [Draine & Hensley 2012, 2013](#)). In our idealized model of DLA dust we focus on silicate and iron-rich species. Silicates have been detected in a small sample of DLA systems ([Kulkarni et al. 2007, 2011](#); [Aller et al. 2012, 2014b](#)). Indirect evidence for iron-rich dust in DLAs was found in our previous study ([Gioannini et al. 2017b](#)). We do not consider carbonaceous dust for two reasons. First, carbonaceous compounds are probably missing in the harsh interstellar conditions typical of DLA galaxies, as suggested by the general lack of the 217.5 nm extinction bump in DLA absorbers ([Wild & Hewett 2005](#); [Vladilo et al. 2006](#); [York et al. 2006](#)). Second, with very few exceptions, carbon column densities are not measurable in DLA systems, either because the C II absorption lines are totally saturated or because they are too faint.

The idealized model of dust grains that we adopt here consists of two components: (1) a mixture of olivines and pyroxenes, which are thought to be dominant among interstellar silicates ([Draine 2003](#); [Henning 2010](#)); (2) an iron-rich species different from silicates. The latter component could be iron in metal form and we call it “metallic” for simplicity, even though our dust grain model does not require a specific assumption on the nature of the iron-rich component: it could be in the form of free-flying particles or of metal inclusions in a silicate matrix ([Jones et al. 2013](#); [Zhukovska et al. 2018](#)). The aim of the grain model is to

calculate the  $(\text{Si}/\text{Fe})_d$  and  $(\text{Mg}/\text{Fe})_d$  ratios according to the chemical formula of each species and the relative proportions of the different species present in the mixture of grains. To derive quantitative expressions in parametric form we follow the notation proposed by [Ueda et al. \(2005\)](#). The chemical formulas of pyroxenes,  $\text{Mg}_x\text{Fe}_{(1-x)}\text{SiO}_3$ , and olivines,  $\text{Mg}_{2y}\text{Fe}_{2(1-y)}\text{SiO}_4$ , are an essential ingredient of this parametrization: each of these two species can be Mg-rich or Fe-rich, depending on the values of the parameters  $x$  and  $y$ . In pyroxenes, the limiting cases  $x = 0$  and  $x = 1$  correspond to ferrosilite and enstatite, respectively, whereas in olivines, the cases  $y = 0$  and  $y = 1$  correspond to fayalite and forsterite, respectively. Assuming that all the Si and Mg atoms in dust form are locked in the mixture of pyroxenes and olivines, we have

$$x = \left( \frac{N_{\text{Mg}}}{N_{\text{Mg}} + N_{\text{Fe}}} \right)_{\text{prx}}^d \quad (17)$$

and

$$y = \left( \frac{N_{\text{Mg}}}{N_{\text{Mg}} + N_{\text{Fe}}} \right)_{\text{olv}}^d, \quad (18)$$

where the quantities  $N_X$  are the column densities of atoms of the element  $X$  locked in dust. The proportion of pyroxenes and olivines in the mixture is specified with the parameter

$$\alpha = \frac{N_{\text{prx}}}{N_{\text{prx}} + N_{\text{olv}}}, \quad (19)$$

where  $N_{\text{prx}} = N[\text{Mg}_x\text{Fe}_{(1-x)}\text{SiO}_3]$  and  $N_{\text{olv}} = N[\text{Mg}_{2y}\text{Fe}_{2(1-y)}\text{SiO}_4]$  are the column densities of pyroxenes and olivine molecules, respectively. With the above parametrization the number of Si and Mg atoms in silicates can be expressed as

$$N_{\text{Si}}^d = N_{\text{prx}} + N_{\text{olv}} \quad (20)$$

**Table 3**  
Parameters of the Dust Grain Composition as Suggested by Observational Studies of the Galactic ISM

$\alpha$	$x$	$y$	$\mu$	Reference	Observation	Interstellar Region
0.2	0.55	0.45	0.00	Kemper et al. (2004)	IR abs.	Galactic center
0.2	0.55	0.45	0.75	Kemper et al. (2004)	IR abs.	Galactic center
0.2	0.50	0.70	0.55	Ueda et al. (2005)	X-ray abs.	Galactic center
0.5	0.71	0.71	0.00	Costantini et al. (2005)	X-ray abs.	Cyg X-2
0.5	0.71	0.71	0.75	Costantini et al. (2005)	X-ray abs.	Cyg X-2
0.5	0.95	0.95	0.00	Min et al. (2007)	IR abs.	Galactic center
0.5	0.95	0.95	0.75	Min et al. (2007)	IR abs.	Galactic center

**Note.** The parameters  $\alpha$ ,  $x$ ,  $y$ , and  $\mu$ , described in Section 4.2, are listed in the first four columns of the table. With the exception of the work by Ueda et al. (2005) the parameter  $\mu$  is not determined by observations and is treated as a free parameter. In the last three columns we report the bibliographic reference, the observational technique used, and the galactic region investigated.

and

$$N_{\text{Mg}}^d = x N_{\text{prx}} + 2y N_{\text{olv}}. \quad (21)$$

Concerning the iron atoms in dust, we assume that they can be incorporated both in silicates and in the “metallic” component. Based on the chemical formula, the number of Fe atoms in silicates is

$$N_{\text{Fe(silicates)}}^d = (1 - x) N_{\text{prx}} + 2(1 - y) N_{\text{olv}}. \quad (22)$$

If we call  $N_{\text{Fe(met)}}$  the number of iron atoms in “metallic” form, the fraction of Fe atoms in this component is

$$\mu = \frac{N_{\text{Fe(met)}}^d}{N_{\text{Fe(met)}}^d + N_{\text{Fe(silicates)}}^d}. \quad (23)$$

The total number of Fe atoms in solid phase,  $N_{\text{Fe}}^d = N_{\text{Fe(met)}}^d + N_{\text{Fe(silicates)}}^d$ , can be expressed as

$$N_{\text{Fe}}^d = \frac{(1 - x)N_{\text{prx}} + 2(1 - y)N_{\text{olv}}}{(1 - \mu)}. \quad (24)$$

From the above definitions the number densities of (Si/Fe) and (Mg/Fe) in the dust phase can be parametrized with the following expressions:

$$\left(\frac{\text{Si}}{\text{Fe}}\right)_d = \frac{(1 - \mu)}{(1 - x)\alpha + 2(1 - y)(1 - \alpha)} \quad (25)$$

and

$$\left(\frac{\text{Mg}}{\text{Fe}}\right)_d = \frac{(1 - \mu)[x\alpha + 2y(1 - \alpha)]}{(1 - x)\alpha + 2(1 - y)(1 - \alpha)}. \quad (26)$$

With these expressions and the proper choice of their parameters we can compare the dust abundance ratios predicted by our idealized mixture of dust grains with the measurements of individual DLAs presented in Section 3. From this comparison we can cast light on the relative proportions of different types of silicates and “metallic” dust, as long as the idealized mixture of grains provides a reasonable description of the dust composition. Before proceeding, we compare our results with studies of the dust abundance ratios (Si, Mg/Fe)<sub>d</sub> in the Milky Way.

#### 4.2.1. Dust Abundance Ratios in the ISM of the Milky Way

Empirical estimates of the parameters  $\alpha$ ,  $x$ ,  $y$ , and  $\mu$  have been obtained in a few interstellar lines of sight of the

Milky Way. Using these estimates we can compare the ratios (Si, Mg/Fe)<sub>d</sub> obtained for DLAs from Equation (5) with the ratios inferred from Equations (25) and (26) for the dust in the Milky Way. The parameters  $\alpha$ ,  $x$ , and  $y$  have been estimated observationally by using IR (Kemper et al. 2004; Min et al. 2007; Fogerty et al. 2016) and X-ray measurements (Costantini et al. 2005; Lee & Ravel 2005; Ueda et al. 2005; Lee 2010). Based on the IR measurements, Kemper et al. (2004) investigated the 10  $\mu\text{m}$  silicate feature in the line of sight of the Galactic center, obtaining a best agreement with observations when a mixture of 15% for pyroxenes and 85% for olivines was adopted in their model. Similar results were confirmed by Fogerty et al. (2016), which suggest a 50/50 abundance of the two species. Ueda et al. (2005), by means of high-resolution X-ray spectroscopy constrained the parameters as  $\alpha = 0.2$ ,  $x = 0.5$ , and  $y = 0.7$ . The same authors estimated a value of 0.45 for the total fraction of Fe in pyroxenes or olivines, which implies  $\mu = 0.55$  for the fraction in metallic form. This is the only estimate of  $\mu$  that can be inferred from the above cited literature. Other estimates can be found in models of dust composition: for instance, a value of 0.7 has been adopted for the fraction of metal inclusions locked into a matrix silicates (Jones et al. 2013). Given the uncertainty on  $\mu$ , we explored a broad range of values, from  $\mu = 0.0$  (all iron in pyroxenes or olivines) up to  $\mu = 0.75$  (most iron in free-flying metal particles or in metal inclusions). We then calculated the ratios (Si, Mg/Fe)<sub>d</sub> for the sets of parameters listed in Table 3, representative of the Milky Way data. The results are shown in form of horizontal lines in Figure 4 where, for the sake of comparison, we overplot the estimates of individual DLAs presented in Section 3 (diamonds with error bars). The set of parameters from Ueda et al. (2005), the only one for which an estimate of  $\mu$  is provided, yields ratios that are in general agreement with the average of individual DLA ratios. For the other lines of sight of the Milky Way, the uncertainty on  $\mu$  leads to a range of results bracketed by the thin lines ( $\mu = 0$ ) and the thick lines ( $\mu = 0.75$ ), the latter ones being characterized by significantly lower (Si, Mg/Fe)<sub>d</sub> ratios. The parameters from Kemper et al. (2004) yield a good agreement with DLAs at high metallicities ( $[\text{Fe}/\text{H}] > -1$ ), but not at low metallicity. With few exceptions, the parameters from Min et al. (2007) yield values of (Si, Mg/Fe)<sub>d</sub> higher than in DLAs at all metallicities. A general agreement is obtained with the grain parameters from Costantini et al. (2005), for which a large fraction of DLA data are contained between the upper ( $\mu = 0$ ) and lower limit ( $\mu = 0.75$ ). It is useful to clarify that, despite the uncertainties in the silicate composition and the fraction of iron in silicates, the high values of Fe depletions

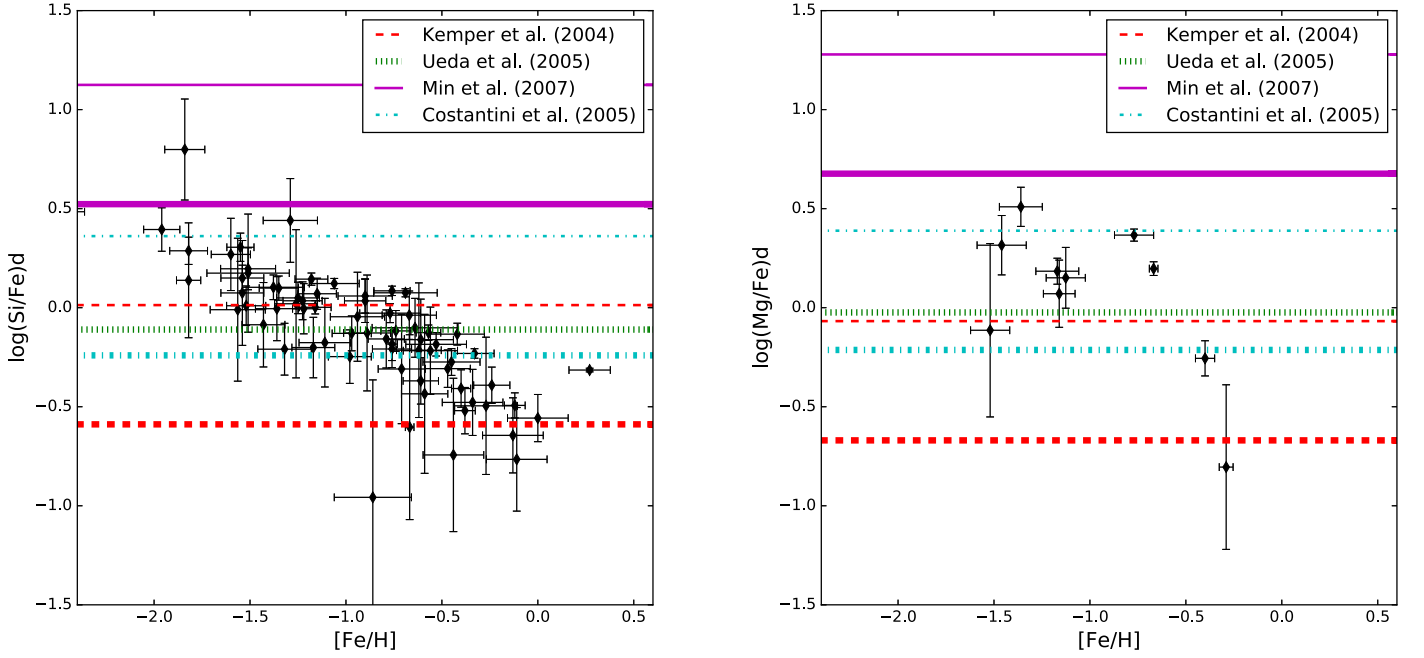


**Figure 4.** Comparison of the dust abundance ratios  $(\text{Si}/\text{Fe})_d$  and  $(\text{Mg}/\text{Fe})_d$  shown in Figure 1 (diamonds with error bars) with estimates of the same ratios in the dust of the Milky Way ISM (horizontal lines). The dust grain parameters of the ISM papers indicated in the box are summarized in Table 3. The thin and thick lines represent values of  $\mu = 0.0$  and  $0.75$ , respectively. See Section 4.2.1.

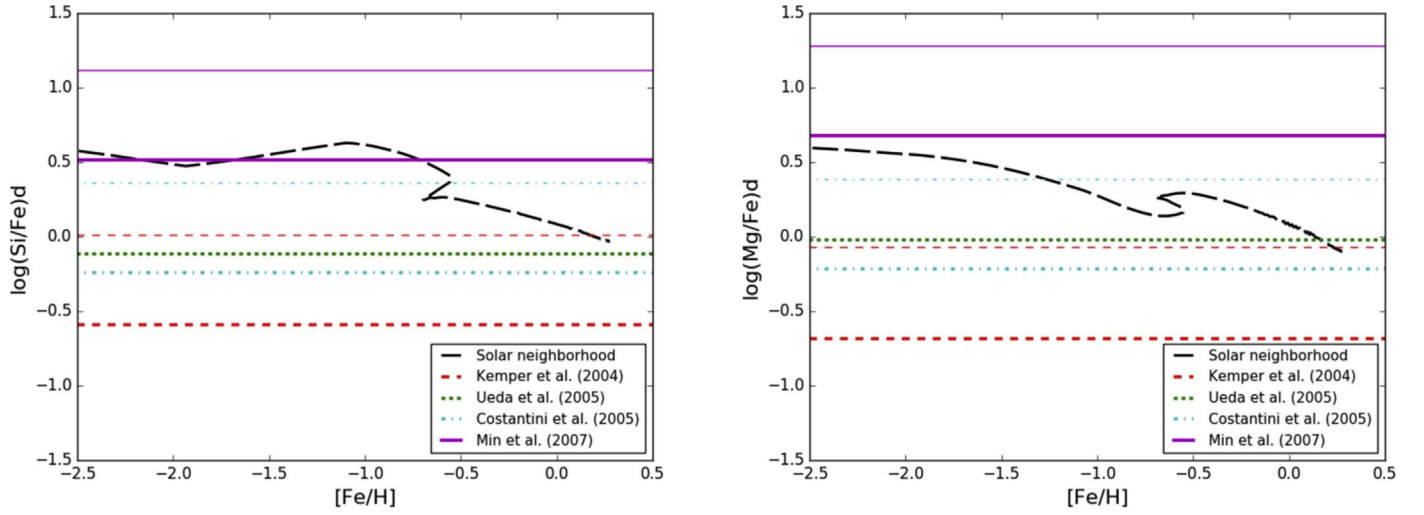


**Figure 5.** Dashed curves: predictions of the  $(\text{Si}/\text{Fe})_d$  and  $(\text{Mg}/\text{Fe})_d$  ratios in the ISM of the solar neighborhood obtained from the Milky Way model of Spitoni et al. (2017). Horizontal lines: empirical estimates of the same ratios in the Milky Way as in Figure 4. See Section 4.2.1.

measured in Mg-rich silicates (Costantini et al. 2005; Min et al. 2007) suggest that the case  $\mu = 0$  can be excluded and that  $\mu$  is probably close to 1 in the Milky Way.

The empirical data described above do not bear information on the evolution of the dust abundance ratios in the Milky Way. To provide insight on this aspect we calculated the evolution of the  $(\text{Si}, \text{Mg}/\text{Fe})_d$  ratios using the Milky Way model of Spitoni et al. (2017), which features the same updated recipes for dust production as in our model. The curve with dashed lines displayed in Figure 5 shows the results obtained for the solar neighborhood. This result predicts the existence of a general decrease of the local interstellar  $(\text{Si}, \text{Mg}/\text{Fe})_d$  ratios in the course of the chemical evolution of the Milky Way. Within the uncertainties of the measurements and of the parameter  $\mu$ , the predicted values of the ratios are in broad agreement with

the empirical estimates. Altogether, the comparison with measurements and models of the Milky Way indicate a general consistency with the behavior of the  $(\text{Si}, \text{Mg}/\text{Fe})_d$  ratios in DLA systems estimated with our method.

The comparison between the Milky Way and DLA results must be interpreted with caution given the different physical conditions that characterize the local and high-redshift interstellar environments. Notwithstanding, recent studies of interstellar depletions have found a continuity of the dust properties in different types of galaxies, including the Milky Way and DLA host galaxies (De Cia et al. 2016; De Cia 2018). The consistency between the DLA ratios estimated with Equation (5) and the local ISM ratios estimated with Equations (25) and (26) lends support to a continuity of dust properties in galaxies of different morphological type. The spread of the  $(\text{Si}, \text{Mg}/\text{Fe})_d$  ratios that

we see in Figure 4 can be explained by differences in the local conditions of the interstellar regions sampled by different lines of sight. In particular, the fact that the QSO line of sight may randomly sample different phases of the ISM can explain the spread observed in DLAs of given metallicity. The values  $(\text{Si}/\text{Fe})_d > 1$  found in DLAs at low metallicity may indicate the peculiarity of dust formation processes in the very early stages of evolution of DLA host galaxies. As we have shown in Section 4.1, the trends with metallicity that we see in DLA systems can be explained in terms of dust formation, accretion, and destruction processes taking place in the course galactic evolution. In the next paragraphs we show that the parametrization introduced in Section 4.2 can be applied to provide a simple model of the evolutionary trends of the  $(\text{Si}, \text{Mg}/\text{Fe})_d$  ratios.

#### 4.2.2. Evolution of the Dust Grain Composition

By adopting a set of metallicity-dependent prescriptions for the parameters  $x$ ,  $y$ , and  $\mu$ , we can use Equations (25) and (26) to model the observed trends with the metallicity of the  $(\text{Si}/\text{Fe})_d$  and  $(\text{Mg}/\text{Fe})_d$  ratios. Concerning the parameters  $x$  and  $y$ , we assume that the relative proportions of Mg and Fe incorporated in silicates will scale with the corresponding proportions of Mg and Fe present in the ISM. Assuming this is true for both pyroxenes and olivines, we obtain the scaling relation

$$x = y = \left( \frac{\text{Mg}}{\text{Mg} + \text{Fe}} \right)_{\text{ISM}}. \quad (27)$$

Accordingly, enstatite and forsterite will be the dominant forms of pyroxenes and olivines when  $(\text{Mg}/\text{Fe})_{\text{ISM}} \gg 1$ , whereas ferrosilite and fayalite will be the dominant forms when  $(\text{Mg}/\text{Fe})_{\text{ISM}} \ll 1$ .

To derive an analytical expression for  $\mu$ , we consider the asymptotic behavior of this quantity in two extreme cases. When  $(\text{Fe}/\text{Si})_{\text{ISM}} \gg 1$  we expect  $\mu \simeq 1$ , i.e., most of solid-phase iron in non-silicate form, because in this case the number of iron atoms in the ISM is much higher than the number that can be accommodated in silicates according to the chemical formula of pyroxenes and olivines. When  $(\text{Si}/\text{Fe})_{\text{ISM}} \gg 1$ , Mg/Fe and O/Fe will also be overabundant in the ISM because Si, Mg, and O share a similar nucleosynthetic history, all of them being  $\alpha$ -capture elements; therefore, when  $(\text{Si}/\text{Fe})_{\text{ISM}} \gg 1$  all the ingredients of silicates will be abundant, with the exception of iron; in this case it is reasonable to assume that  $\mu \simeq 0$ , because the small number of iron atoms will be sequestered by silicates, with virtually no iron atoms available to form the “metallic” dust component. Based on these considerations we adopt the simple analytical expression

$$\mu = \frac{1}{1 + (\text{Si}/\text{Fe})_{\text{ISM}}}, \quad (28)$$

which yields the asymptotic values  $\mu \simeq 0$  when  $(\text{Si}/\text{Fe})_{\text{ISM}} \gg 1$  and  $\mu \simeq 1$  when  $(\text{Fe}/\text{Si})_{\text{ISM}} \gg 1$ .

To introduce the metallicity dependence in Equations (27) and (28), we adopt the ISM abundances of Si, Mg, and Fe predicted by the galactic evolution model described in Section 2.2. Since these ISM abundances refer to the total number of atoms (gas plus dust), with no distinction between the gas and solid phase, the evolutionary trends that we obtain from Equations (27) and (28) are unrelated to the model

predictions shown in Figure 3, which are instead based on the recipes of dust production described in Section 4.1.

In the addition of  $x$ ,  $y$ , and  $\mu$ , Equations (25) and (26) also require an estimate of  $\alpha$ . In lack of a prescription for the relative proportions of pyroxenes and olivines in the ISM, we treat  $\alpha$  as a free parameter. We note that, thanks to the simplified assumption  $x = y$  of Equation (27), the  $(\text{Mg}/\text{Fe})_d$  ratio is independent of  $\alpha$ . In fact assuming  $x = y$  Equation (26) becomes

$$\left( \frac{\text{Mg}}{\text{Fe}} \right)_d = \frac{(1 - \mu)x}{(1 - x)}. \quad (29)$$

Therefore, only the  $(\text{Si}/\text{Fe})_d$  will depend on the choice of  $\alpha$ .

The curves in Figure 6 show the metallicity evolution of the  $(\text{Si}/\text{Fe})_d$  and  $(\text{Mg}/\text{Fe})_d$  ratios predicted by inserting Equations (25) and (26) in (27) and (28). The curves in the left panel of the figure show the  $(\text{Si}/\text{Fe})_d$  ratio for the different values of  $\alpha$  indicated in the legend. The curve in the right panel represents the metallicity evolution of  $(\text{Mg}/\text{Fe})_d$ , which is independent of  $\alpha$ , as shown in Equation (29). In both panels of the figure the curves are in general agreement with the indirect measurements presented in Section 3 (diamonds with error bars): as the metallicity increases, the  $(\text{Si}/\text{Fe})_d$  and  $(\text{Mg}/\text{Fe})_d$  ratios decrease, i.e., the contribution of iron to interstellar dust becomes more prominent, with an increasing presence of iron in non-silicate, possibly metallic form. The fact that the dust grain model of  $(\text{Mg}/\text{Fe})_d$  tracks reasonably well the (small) data sample is rather remarkable, considering that the  $(\text{Mg}/\text{Fe})_d$  model is fixed by Equations (26)–(28) without any free parameter. Concerning the  $(\text{Si}/\text{Fe})_d$  ratio, the curves of the model shift to lower values of the ratio as  $\alpha$  decreases. The curves with high values of  $\alpha$  lie above most of the data, those with  $\alpha \simeq 0$  yield the best agreement: the silicate composition appears to be dominated by olivines rather than pyroxenes. The comparison of  $(\text{Si}/\text{Fe})_d$  ratios derived from different models of chemical evolution (Figure 2) suggests that systematic uncertainties are generally smaller than the variations predicted for different values of  $\alpha$ .

The relative abundance of olivines and pyroxenes that we infer can be compared with previous results on the composition of silicate grains. From a comparison between new laboratory measurements of silicate compounds and a silicate absorption feature in the line of sight of an X-ray binary, Zeegers et al. (2017) found a best fit to the data when the interstellar dust is dominated by olivines. From the analysis of the silicate composition in 93 active galactic nuclei, Xie et al. (2017) found general evidence for a mixture of pyroxenes and olivines or a pure olivine composition; only in two cases evidence was found for a pure pyroxene mixture. The properties of the silicate features at  $13 \mu\text{m}$  (Aller et al. 2014a, 2014b) and  $9.7 \mu\text{m}$  (Kulkarni et al. 2007) were investigated in the spectra of QSO absorbers, which represent an environment similar to the one studied here. Aller et al. (2014a) found a general agreement between models and observations when an olivine-rich dust composition is adopted, even if they found variations in different absorbers, which may indicate the existence of differences in the silicate grain properties between different absorbers. Summarizing the above results, we can conclude that the predominance of olivines that we found as shown in the left panel of Figure 6 is in line with previous results on the composition of silicate grains in several different environments.

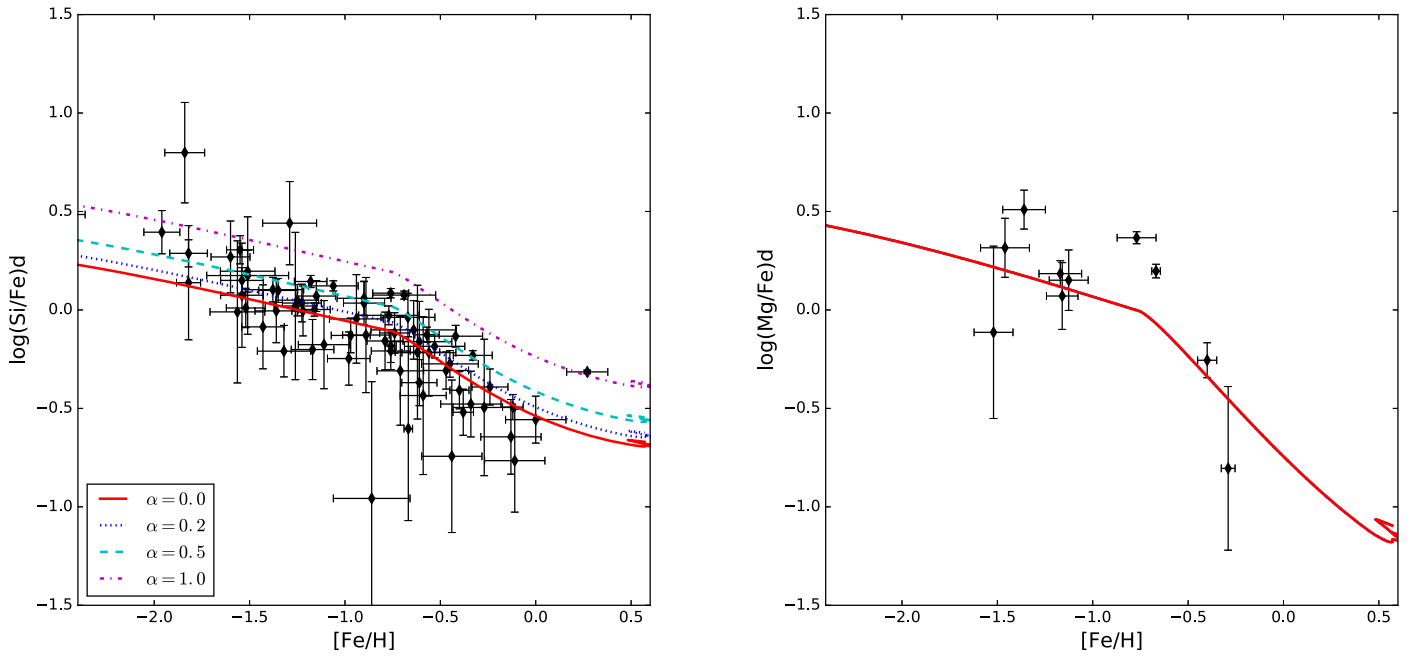


**Figure 6.** Comparison of the dust abundance ratios  $(\text{Si}/\text{Fe})_d$  and  $(\text{Mg}/\text{Fe})_d$  shown in Figure 1 (diamonds with error bars) with the predictions of a simple evolutionary model of dust grain composition (Section 4.2.2). The different lines in the left panel represent the predicted evolution of the  $(\text{Si}/\text{Fe})_d$  ratio at constant values of  $\alpha$ , as indicated in the legend. The curve in the right panel shows the predicted evolution of the  $(\text{Mg}/\text{Fe})_d$  ratio, which is independent of  $\alpha$ , as shown in Equation (29).

## 5. Conclusions

We have presented a method to estimate the relative abundances of refractory elements incorporated in the dust phase of DLA absorbers. The method is based on the synergy between measurements of gas-phase column densities and predictions of total ISM abundances (gas plus dust) obtained from models of galactic chemical evolution previously tuned for DLA systems. We have applied the method to obtain indirect measurements of the dust abundance ratios  $(\text{Si}/\text{Fe})_d$  and  $(\text{Mg}/\text{Fe})_d$  for a sample of DLA systems spanning a broad range of metallicities. These data provide a unique tool for probing the dust grain composition of galaxies observed in different stages of their evolution and therefore to probe evolutionary trends of dust chemical composition. From the analysis of these data we find the following results:

1. The dust-phase abundance ratios  $(\text{Si}/\text{Fe})_d$  and  $(\text{Mg}/\text{Fe})_d$  decrease significantly in the course of chemical evolution, namely, by almost two orders of magnitude in the metallicity interval from  $\simeq 1/100$  solar to approximately solar. This decrease is much stronger than the well-known decrease of  $\alpha/\text{Fe}$  ratios found in studies of metal-poor stars and galaxies (including DLA host galaxies), which is generally smaller than half an order of magnitude.
2. To cast light on the evolutionary trend of the dust composition that we found, we investigated the potential contribution of stellar sources and interstellar processes to the cycle of dust production. We find that the evolution of the  $(\text{Si}/\text{Fe})_d$  and  $(\text{Mg}/\text{Fe})_d$  ratios is governed by different dust processes at low and high metallicity. At low metallicities ( $[\text{Fe}/\text{H}] < -0.6$ ), Type II SNe represent the most important source, whereas at higher metallicities dust accretion is the most important process. Our analysis suggests the existence of Fe-rich dust, possibly in

metallic form, which preferably forms by accretion in the ISM rather than in stellar ejecta.

3. To further investigate the nature of the dust in DLA absorbers, we adopted an idealized model of dust grains consisting of a mixture of silicates, with variable proportions of pyroxenes and olivines, and an iron-rich species different from silicates. By parameterizing the relative amounts of these different constituents, the dust grain model provides quantitative estimates of  $(\text{Si}/\text{Fe})_d$  and  $(\text{Mg}/\text{Fe})_d$  ratios. The Galactic interstellar estimates of these ratios show a general consistency with the indirect measurements of the same ratios in DLA systems. The analysis of these data suggests that the adopted mixture of silicates and iron-rich dust represents a reasonable model for the composition of dust grains in DLA absorbers, with the contribution of the iron-rich component becoming more important in the course of galactic chemical evolution.
4. By introducing a metallicity dependence in the parameters that fix the proportions of the different constituents of dust grains, we were able to reproduce the observed evolutionary trends of the  $(\text{Si}/\text{Fe})_d$  and  $(\text{Mg}/\text{Fe})_d$  ratios in DLA systems. The  $(\text{Si}/\text{Fe})_d$  trend is best reproduced assuming that olivines dominate over pyroxenes. This result is in line with previous studies of interstellar dust, which suggest that among interstellar silicates, olivines are more common than pyroxenes.

This study confirms the remarkable capability of DLA absorbers to probe the evolutionary properties of high-redshift galaxies. By enlarging the sample of DLA column-density measurements, the application of the method presented here will improve our understanding of the nature and evolution of interstellar dust in the distant universe.

We thank Emanuele Spitoni for important suggestions concerning the evolution of dust in the Milky Way and Marco

Fulle for helpful discussions on the possible fate of free-flying iron particles once incorporated in the solar nebula. The suggestions provided by an anonymous reviewer significantly improved the presentation of this work.

### ORCID iDs

Giovanni Vladilo  <https://orcid.org/0000-0001-7604-8332>  
 Francesca Matteucci  <https://orcid.org/0000-0001-7067-2302>

### References

- Agladze, N. I., Sievers, A. J., Jones, S. A., Burlitch, J. M., & Beckwith, S. V. W. 1996, *ApJ*, **462**, 1026
- Aller, M. C., Kulkarni, V. P., York, D. G., et al. 2012, *ApJ*, **748**, 19
- Aller, M. C., Kulkarni, V. P., York, D. G., et al. 2014a, arXiv:1405.0426
- Aller, M. C., Kulkarni, V. P., York, D. G., et al. 2014b, *ApJ*, **785**, 36
- Asano, R. S., Takeuchi, T. T., Hirashita, H., & Nozawa, T. 2013, *MNRAS*, **432**, 637
- Asplund, M., Grevesse, N., Sauval, A. J., & Scott, P. 2009, *ARA&A*, **47**, 481
- Bielby, R., Crighton, N. H. M., Fumagalli, M., et al. 2017, *MNRAS*, **468**, 1373
- Blair, W. P., Ghavamian, P., Long, K. S., et al. 2007, *ApJ*, **662**, 998
- Bouché, N., Murphy, M. T., Péroux, C., et al. 2012, *MNRAS*, **419**, 2
- Bradamante, F., Matteucci, F., & D'Ercole, A. 1998, *A&A*, **337**, 338
- Calura, F., Matteucci, F., & Vladilo, G. 2003, *MNRAS*, **340**, 59
- Calura, F., Pipino, A., & Matteucci, F. 2008, *A&A*, **479**, 669
- Christensen, L., Møller, P., Fynbo, J. P. U., & Zafar, T. 2014, *MNRAS*, **445**, 225
- Cooke, R., Pettini, M., Steidel, C. C., Rudie, G. C., & Nissen, P. E. 2011, *MNRAS*, **417**, 1534
- Cooke, R. J., Pettini, M., & Jorgenson, R. A. 2015, *ApJ*, **800**, 12
- Cooke, R. J., Pettini, M., & Steidel, C. C. 2017, *MNRAS*, **467**, 802
- Costantini, E., Freyberg, M. J., & Predehl, P. 2005, *A&A*, **444**, 187
- Coupeaud, A., Demyk, K., Meny, C., et al. 2011, *A&A*, **535**, A124
- De Cia, A. 2018, *A&A*, **613**, L2
- De Cia, A., Ledoux, C., Mattsson, L., et al. 2016, *A&A*, **596**, A97
- De Cia, A., Ledoux, C., Savaglio, S., Schady, P., & Vreeswijk, P. M. 2013, *A&A*, **560**, A88
- Desert, F.-X., Boulanger, F., & Puget, J. L. 1990, *A&A*, **237**, 215
- Draine, B. T. 2003, *ARA&A*, **41**, 241
- Draine, B. T., & Hensley, B. 2012, *ApJ*, **757**, 103
- Draine, B. T., & Hensley, B. 2013, *ApJ*, **765**, 159
- Draine, B. T., & Lee, H. M. 1984, *ApJ*, **285**, 89
- Dwek, E. 1998, *ApJ*, **501**, 643
- Dwek, E. 2004, *ApJL*, **611**, L109
- Dwek, E. 2016, *ApJ*, **825**, 136
- Fogarty, S., Forrest, W., Watson, D. M., Sargent, B. A., & Koch, I. 2016, *ApJ*, **830**, 71
- François, P., Matteucci, F., Cayrel, R., et al. 2004, *A&A*, **421**, 613
- Fumagalli, M., Haardt, F., Theuns, T., et al. 2017, *MNRAS*, **467**, 4802
- Fumagalli, M., O'Meara, J. M., Prochaska, J. X., Rafelski, M., & Kanekar, N. 2015, *MNRAS*, **446**, 3178
- Fynbo, J. P. U., Laursen, P., Ledoux, C., et al. 2010, *MNRAS*, **408**, 2128
- Gioannini, L., Matteucci, F., & Calura, F. 2017a, *MNRAS*, **471**, 4615
- Gioannini, L., Matteucci, F., Vladilo, G., & Calura, F. 2017b, *MNRAS*, **464**, 985
- Gomez, H. L., Clark, C. J. R., Nozawa, T., et al. 2012, *MNRAS*, **420**, 3557
- Henning, T. 2010, *ARA&A*, **48**, 21
- Hollenbach, D., & Salpeter, E. E. 1971, *ApJ*, **163**, 155
- Hou, J. L., Boissier, S., & Prantzos, N. 2001, in *Cosmic Evolution*, ed. E. Vangioni-Flam, R. Ferlet, & M. Lemione (Hackensack, NJ: World Scientific), 297
- Hoyle, F., & Wickramasinghe, N. C. 1969, *Natur*, **223**, 459
- Iwamoto, K., Brachwitz, F., Nomoto, K., et al. 1999, *ApJS*, **125**, 439
- Jenkins, E. B. 2009, *ApJ*, **700**, 1299
- Jenkins, E. B. 2014, arXiv:1402.4765
- Jones, A. 2014, arXiv:1411.6666
- Jones, A. P., Fanciullo, L., Köhler, M., et al. 2013, *A&A*, **558**, A62
- Junkkarinen, V. T., Cohen, R. D., Beaver, E. A., et al. 2004, *ApJ*, **614**, 658
- Keller, L. P., Hony, S., Bradley, J. P., et al. 2002, *Natur*, **417**, 148
- Kemper, F., Vriend, W. J., & Tielens, A. G. G. M. 2004, *ApJ*, **609**, 826
- Krogager, J.-K., Fynbo, J. P. U., Ledoux, C., et al. 2013, *MNRAS*, **433**, 3091
- Kulkarni, V. P., Torres-Garcia, L. M., Som, D., et al. 2011, *ApJ*, **726**, 14
- Kulkarni, V. P., Woodgate, B. E., York, D. G., et al. 2006, *ApJ*, **636**, 30
- Kulkarni, V. P., York, D. G., Vladilo, G., & Welty, D. E. 2007, *ApJL*, **663**, L81
- Kunth, D., Matteucci, F., & Marconi, G. 1995, *A&A*, **297**, 634
- Le Brun, V., Bergeron, J., & Deharveng, J. M. 1997, *A&A*, **321**, 733
- Lee, J. C. 2010, *SSRv*, **157**, 93
- Lee, J. C., & Ravel, B. 2005, *ApJ*, **622**, 970
- Li, A., & Draine, B. T. 2001, *ApJ*, **554**, 778
- Lodders, K. 2003, *ApJ*, **591**, 1220
- Lu, L., Sargent, W. L. W., Womble, D. S., & Barlow, T. A. 1996, *ApJL*, **457**, L1
- Mathis, J. S. 1990, *ARA&A*, **28**, 37
- Mathis, J. S., Rumpl, W., & Nordsieck, K. H. 1977, *ApJ*, **217**, 425
- Matteucci, F. 2001a, *The Chemical Evolution of the Galaxy*, Astrophysics and Space Science Library, Vol. 253 (Dordrecht: Kluwer Academic)
- Matteucci, F. 2001b, *Chemical Evolution of Galaxies* (Berlin: Springer)
- Matteucci, F., Molaro, P., & Vladilo, G. 1997, *A&A*, **321**, 45
- Matteucci, F., & Recchi, S. 2001, *ApJ*, **558**, 351
- Mennella, V., Brucato, J. R., Colangeli, L., et al. 1998, *ApJ*, **496**, 1058
- Min, M., Waters, L. B. F. M., de Koter, A., et al. 2007, *A&A*, **462**, 667
- Møller, P., & Warren, S. J. 1998, *MNRAS*, **299**, 661
- Noterdaeme, P., Laursen, P., Petitjean, P., et al. 2012, *A&A*, **540**, A63
- Nozawa, T., Maeda, K., Kozasa, T., et al. 2011, *ApJ*, **736**, 45
- Padovani, P., & Matteucci, F. 1993, *ApJ*, **416**, 26
- Pagel, B. E. J. 2009, *Nucleosynthesis and Chemical Evolution of Galaxies* (Cambridge: Cambridge Univ. Press)
- Péroux, C., Bouché, N., Kulkarni, V. P., York, D. G., & Vladilo, G. 2011, *MNRAS*, **410**, 2237
- Piovani, L., Chiosi, C., Merlin, E., et al. 2011, arXiv:1107.4541
- Pollack, J. B., Hubickyj, O., Bodenheimer, P., et al. 1996, *Icar*, **124**, 62
- Prochaska, J. X., Gawiser, E., Wolfe, A. M., Castro, S., & Djorgovski, S. G. 2003, *ApJL*, **595**, L9
- Rafelski, M., Wolfe, A. M., Prochaska, J. X., Neeleman, M., & Mendez, A. J. 2012, *ApJ*, **755**, 89
- Rahmani, H., Péroux, C., Augustin, R., et al. 2018, *MNRAS*, **474**, 254
- Rao, S. M., Nestor, D. B., Turnshek, D. A., et al. 2003, *ApJ*, **595**, 94
- Recchi, S., Matteucci, F., & D'Ercole, A. 2002, in *ASP Conf. Proc.* 253, *Chemical Enrichment of Intracluster and Intergalactic Medium*, ed. R. Fusco-Femiano & F. Matteucci (San Francisco, CA: ASP), 397
- Safronov, V. S., & Zvjagina, E. V. 1969, *Icar*, **10**, 109
- Salpeter, E. E. 1955, *ApJ*, **121**, 161
- Salvadori, S., & Ferrara, A. 2012, *MNRAS*, **421**, L29
- Savage, B. D., & Sembach, K. R. 1996, *ARA&A*, **34**, 279
- Schmidt, M. 1959, *ApJ*, **129**, 243
- Sofia, U. J., Gordon, K. D., Clayton, G. C., et al. 2006, *ApJ*, **636**, 753
- Spitoni, E., Gioannini, L., & Matteucci, F. 2017, *A&A*, **605**, 38
- Spitoni, E., Matteucci, F., Recchi, S., Cescutti, G., & Pipino, A. 2009, *A&A*, **504**, 87
- Spitoni, E., Vincenzo, F., Matteucci, F., & Romano, D. 2016, *MNRAS*, **458**, 2541
- Spitzer, L., Jr., & Jenkins, E. B. 1975, *ARA&A*, **13**, 133
- Ueda, Y., Mitsuda, K., Murakami, H., & Matsushita, K. 2005, *ApJ*, **620**, 274
- van den Hoek, L. B., & Groenewegen, M. A. T. 1997, *A&AS*, **123**, 305
- Vladilo, G. 1998, *ApJ*, **493**, 583
- Vladilo, G. 2002, *ApJ*, **569**, 295
- Vladilo, G., Abate, C., Yin, J., Cescutti, G., & Matteucci, F. 2011, *A&A*, **530**, A33
- Vladilo, G., Centurión, M., Bonifacio, P., & Howk, J. C. 2001, *ApJ*, **557**, 1007
- Vladilo, G., Centurión, M., Levshakov, S. A., et al. 2006, *A&A*, **454**, 151
- Voshchinnikov, N. V., & Henning, T. 2010, *A&A*, **517**, A45
- Whelan, J., & Iben, I., Jr. 1973, *ApJ*, **186**, 1007
- Wickramasinghe, N. C., & Wickramasinghe, A. N. 1993, *Ap&SS*, **200**, 145
- Wild, V., & Hewett, P. 2005, *MNRAS*, **361**, L30
- Wild, V., Hewett, P., & Pettini, M. 2006, *MNRAS*, **367**, 211
- Williams, B. J., Borkowski, K. J., Reynolds, S. P., et al. 2012, *ApJ*, **755**, 3
- Wolfe, A. M., Gawiser, E., & Prochaska, J. X. 2005, *ARA&A*, **43**, 861
- Wolfe, A. M., Turnshek, D. A., Smith, H. E., & Cohen, R. D. 1986, *ApJS*, **61**, 249
- Xie, Y., Li, A., & Hao, L. 2017, *ApJS*, **228**, 6
- York, D. G., Khare, P., Vanden Berk, D., et al. 2006, *MNRAS*, **367**, 945
- Zeegers, S. T., Costantini, E., de Vries, C. P., et al. 2017, *A&A*, **599**, A117
- Zhukovska, S. 2014, *A&A*, **562**, A76
- Zhukovska, S., Gail, H.-P., & Tieloff, M. 2008, *A&A*, **479**, 453
- Zhukovska, S., Henning, T., & Dobbs, C. 2018, *ApJ*, **857**, 94
- Zolensky, M. E., Zega, T. J., Yano, H., et al. 2006, *Sci*, **314**, 1735